

# Genetic Algorithm Optimized Robust Nonlinear Observer for a Wind Turbine System Based on Permanent Magnet Synchronous Generator

Mohamed Mansouri<sup>a\*</sup>, Mohamed Bey<sup>a</sup>, Said Hassaine<sup>a</sup>, Mhamed Larbi<sup>a</sup>, Tayeb Allaoui<sup>a</sup>, Mouloud Denai<sup>b</sup>

mohamed.mansouri@univ-tiaret.dz, mohamed.bey@univ-tiaret.dz, s\_hassaine@yahoo.fr, larbi\_mh@yahoo.fr,  
allaoui\_tb@yahoo.fr, m.denai@herts.ac.uk

<sup>a</sup> Laboratory of Energy Engineering and Computer Engineering, IBN Khaldoun University, Tiaret, Algeria.

<sup>b</sup> School of Physics, Engineering and Computer Science, University of Hertfordshire, Hatfield, UK

## Abstract

This paper presents an optimal control scheme for a Permanent Magnet Synchronous Generator (PMSG) coupled to a wind turbine operating without a position sensor. This sensorless scheme includes two observers: The first observer uses the flux to estimate the speed. However, an increase in the temperature or a degradation of the permanent magnet characteristics will result in a demagnetization of the machine causing a drop in the flux. The second observer is therefore used to estimate these changes in the flux from the speed and guarantees the stability of the system. This structure leads to a better exchange of information between the two observers, eliminates the problem of encoder and compensates for the demagnetization problem. To improve the precision of the speed estimator, the gain of the non-linear observer is optimized using Genetic Algorithm (GA) and the speed is obtained from a modified Phase Locked Loop (PLL) method using an optimized Sliding Mode Controller (SMC). Furthermore, to enhance the convergence speed of this observer scheme and improve the performance of the system a Fast Super Twisting Sliding Mode Control (FSTSMC) is introduced to reinforce the SMC strategy. A series of simulations are presented to show the effectiveness and robustness of proposed observer scheme.

**Keywords:** Wind turbine, Non-salient pole PMSG, sensorless control, PLL, genetic algorithm, fast super twisting sliding mode control.

## Introduction

Electric power generation from wind has grown rapidly in the past decade to become the mainstream renewable energy source worldwide. Today, there are several wind turbine technologies in the market with different generator configurations. Permanent Magnet Synchronous Generators are becoming very attractive for full-power conversion and variable-speed wind power applications due to their several advantages including high efficiency and reliability. However, PMSGs are still high cost due to the permanent magnet materials.

Several works have focused on the design of sensorless control of PMSGs to reduce the global cost of a wind energy system and its size [1]. Sensorless control requires an accurate information on the position in order to achieve optimal performance. Several sensorless control methods have been developed and applied. Among these, the Sliding Mode Observer (SMO) has been widely used [2]. This observer is robust but its main drawback is the chattering phenomenon which causes energy losses. The Higher-Order Sliding Mode Observer (HOSMO) has been proposed as an effective approach to reduce chattering [3]. However, HOSMO requires an accurate gain value to achieve a good compromise between chattering, stability, and robustness. Other robust sensorless schemes

based on nonlinear observer have been proposed [4]. A great deal of work addressing the implementation of these types of observers in Permanent Magnet Synchronous Machines (PMSM) can be found in [5-8]. The results have shown that these observers lead to a slow transient response. These types of observers are based on permanent magnet flux and several methods exist to determine this parameter [9]. The simultaneous estimation of the flux and the position simultaneously is a complex task, therefore, an appropriate arrangement of two observers is generally adopted to provide an accurate estimation [10, 11, 12]. In [10], the authors used the Model Reference Adaptive System (MRAS) strategy to estimate the speed and the Extended Kalman Filter (EKF) to extract the flux of the Interior Permanent Magnet Synchronous Motor (IPMSM) and solve the demagnetization problem. However, the long computation time of the EKF and the lack of stability of the MRAS scheme are the major drawbacks of this approach. The authors in [11] proposed a stator flux soft sensor with sensorless speed and applied it to reluctance machines. A formulation of EKF is proposed to extract the flux with speed of PMSM in [12].

To reduce the impact of uncertainties in the system an optimal sensorless control scheme should be designed. Optimization techniques have been extensively used in control system design. Optimization is the task of searching for the parameter value(s) that minimize or maximize a given objective function. The most popular optimization techniques include stochastic or deterministic algorithms [13], the conjugate gradient algorithm [14], and heuristic approaches such as Genetic Algorithm (GA) [15] and Particle Swarm Optimization (PSO) [16].

Evolutionary algorithms (EA) are stochastic methods of global optimization based on the Darwinian theory of the evolution of biological species [17]. The evolution is modeled independently in different ways. Primarily, the GA is developed in [18], which formalizes genetic algorithms in the context of mathematical optimization. In [19], the authors established the Evolutionary Strategies (ESs). An alternative description of evolution programming (EP) has been introduced by Fogel [20].

Several works have used GA to optimize the parameters of controllers such as the gains of the Proportional Integral Derivative (PID) controller [21]. An optimization method is applied to Sliding Mode Control (SMC) [22, 23]. In [22], GA is used to optimize the sliding mode of the variable structure system. In [23], an optimal SMC is used to accurately control the position of an exoskeleton,

The study in [24] proposes the application of an optimized SMC with a nonlinear disturbance observer to stabilize an inverted pendulum. In [25], Genetic Adaptive Observer (GAO) is proposed. The authors in [26], proposed a new adaptive observer scheme to improve global optimality of estimation. In [27], the authors used GA to optimize the observer's parameters for an induction motor drive [27]. The authors in [28] uses GA to select the gains of a sliding mode observer for a Brushless DC (BLDC) motor. These works, despite the important results obtained, were always lacking in the optimal values for the observer and controller which provide more stability to the system.

Based on these works and in order to enhance the stability of the overall system and eliminate the demagnetization problem due to a temperature increase or the permanent magnet flux degradation in the PMSG driven by the wind turbine, the present study aims to design an accurate sensorless control scheme using a two-observer configuration. These dual observers operate simultaneously and exchange information on the speed and flux. The speed observer provides the rotor position, while the speed is obtained through the proposed Phase Locked Loop (PLL) based on the estimated rotor position. The PLL is controlled using SMC the gain of which is optimized using GA to reduce the well-known chattering phenomenon while maintaining a good compromise between precision and speed of response. Furthermore, to obtain an accurate estimate of the position, GA is used to determine the optimal gain of

the speed observer providing a good compromise between steady-state error and response time. The flux observer then uses this speed to identify the permanent magnet flux and passes it on to speed observer thus to FSTSMC. The FSTSMC has been selected first to improve the convergence using field-oriented control theory and second, since it belongs to the family of super twisting SMCs, it will reduce the chattering. The simulation results have shown that the proposed sensorless scheme provides an improved transient response of the speed and flux.

The remaining of the paper is organized as follows. Section 2 presents the mathematical model of the wind turbine and the PMSG. In Section 3, the stator-side control is derived. The proposed sensorless scheme is presented in Section 4. In Section 5, the simulation results are presented and discussed in detail. Finally, the conclusions of this work are summarized in Section 6.

## 2. Modeling of the Wind Energy Conversion System

The structure of the Wind Energy Conversion System (WECS) considered in this work consists of a three-blade wind turbine coupled to the PMSG. The WECS is integrated to the grid through back-to-back converters connected via a DC link [29].

### 2.1 Wind turbine model

The mechanical power of the wind turbine is given by:

$$P_m = \frac{1}{2} C_p(\lambda) \rho \pi R^2 V_w^3 \quad (1)$$

Where  $V_w$  is the wind speed (m/s),  $R$  is the blade radius (m),  $\rho$  is the air density (kg/m<sup>3</sup>),  $C_p$  is the power coefficient and  $\lambda$  is the tip speed ratio which is given by:

$$\lambda = \frac{\omega R}{V_w} \quad (2)$$

The mechanical torque  $\mathcal{T}_m$  is written as follows:

$$\mathcal{T}_m = \frac{P_m}{\omega} = \frac{1}{2} C_p(\lambda, \beta) \rho \pi R^2 V_w^3 \frac{1}{\omega} \quad (3)$$

The value of  $C_p$  is a function of the tip speed ratio ( $\lambda$ ) and the blades pitch angle ( $\beta$ ) [30].

$$C_p = c_1 \left( \frac{c_2}{\lambda_i} - c_3 \beta - c_4 \right) e^{-\frac{c_5}{\lambda_i}} + c_6 \lambda \quad (4)$$

$$\frac{1}{\lambda_i} = \frac{1}{\lambda + 0.08\beta} - \frac{0.035}{\beta^3 + 1} \quad (5)$$

Where  $c_1 = 0.22$ ,  $c_2 = 116$ ,  $c_3 = 0.4$ ,  $c_4 = 5$ ,  $c_5 = 12.5$ ,  $c_6 = 0$ . When  $\beta = 0$  and  $\lambda_{opt} = 6.1$  then  $C_p = 0.38$ .

The gearbox mounted between the wind turbine and the generator is represented by the following equations [31]:

$$\begin{cases} \omega_t = \frac{1}{G} \omega \\ \mathcal{T}_g = \frac{1}{G} \mathcal{T}_t \end{cases} \quad (6)$$

Where  $G$  is the gear ratio,  $\mathcal{T}_g$  and  $\mathcal{T}_t$  are the generator and wind turbine torques respectively.

### 2.2 PMSG model

The PMSG voltage equation in the phasor notation is expressed as:

$$L \frac{di_s}{dt} = -(R_s \mathcal{J} + n_p \omega_r L_s \mathfrak{S}) i_s - n_p \omega_r \Psi_{pm} \mathfrak{S} \xi_s + u_s \quad (7)$$

Where  $u_s$  is the stator voltage,  $R_s$  is the stator resistance,  $L_s$  denotes the stator inductance,  $i_s$  is the stator current,  $n_p$  is the number of pole pairs,  $\omega_r$ ,  $\theta_r$  and  $\psi_{pm}$  are the rotor speed, rotor position and permanent magnet flux linkage respectively [32].

Where  $e^{\tilde{\zeta}\theta_r} = \begin{bmatrix} \cos\theta_r & -\sin\theta_r \\ \sin\theta_r & \cos\theta_r \end{bmatrix}$ , and  $\xi_s = e^{-\tilde{\zeta}\theta_r} \begin{bmatrix} \cos\theta_r \\ \sin\theta_r \end{bmatrix} = \begin{bmatrix} 1 \\ 0 \end{bmatrix}$ .

Where  $\tilde{\zeta}$  is the matrix equivalent to  $\tilde{\zeta}^2 = -1$ ,  $\tilde{\zeta}$  is defined as:  $\tilde{\zeta} = \begin{bmatrix} 0 & -1 \\ 1 & 0 \end{bmatrix}$ , where  $e^{-\tilde{\zeta}\theta}$  : is the (d, q) transformation matrix [33].

The current can be determined from the flux as follows:

$$i_s = L_s^{-1}(\psi_s - \psi_{pm}) = \begin{bmatrix} i_d \\ i_q \end{bmatrix} \quad (8)$$

The inductance matrix is defined as:

$$L_s = e^{-\theta_r\tilde{\zeta}} \begin{bmatrix} L_d & 0 \\ 0 & L_q \end{bmatrix} e^{\theta_r\tilde{\zeta}} \quad (9)$$

The stator flux is given by:

$$\psi_s = \begin{bmatrix} \psi_d \\ \psi_q \end{bmatrix} = \begin{bmatrix} L_d i_d + \psi_{pm} \\ L_q i_q \end{bmatrix} \quad (10)$$

The permanent magnet flux is:

$$\psi_{pm} = e^{-\theta_r\tilde{\zeta}} \begin{bmatrix} \psi_{pm} \\ 0 \end{bmatrix} \quad (11)$$

The mechanical equation of the wind turbine is given by :

$$J \frac{d\omega_r}{dt} = n_p \psi_{pm} i_{\alpha\beta}^T \tilde{\zeta} \begin{bmatrix} \cos\theta_r \\ \sin\theta_r \end{bmatrix} - \Gamma_L - f\omega_r \quad (12)$$

Where  $J$  is the inertia,  $\Gamma_L$ ,  $f$  are the mechanical torque and the viscous friction respectively [34].

The electromagnetic torque can be written as [33, 34]:

$$\Gamma_{em} = n_p \psi_{pm} i_{\alpha\beta}^T \tilde{\zeta} \begin{bmatrix} \cos\theta_r \\ \sin\theta_r \end{bmatrix} \quad (13)$$

### 3. Stator Side Control System

Vector control of the PMSG is implemented as shown in Fig. 1. This includes both the control part and the observer part. The speed is determined from the sensorless block. The d-axis current component must follow the zero reference, while the reference current of the q-axis is obtained from the speed control loop [3, 35].

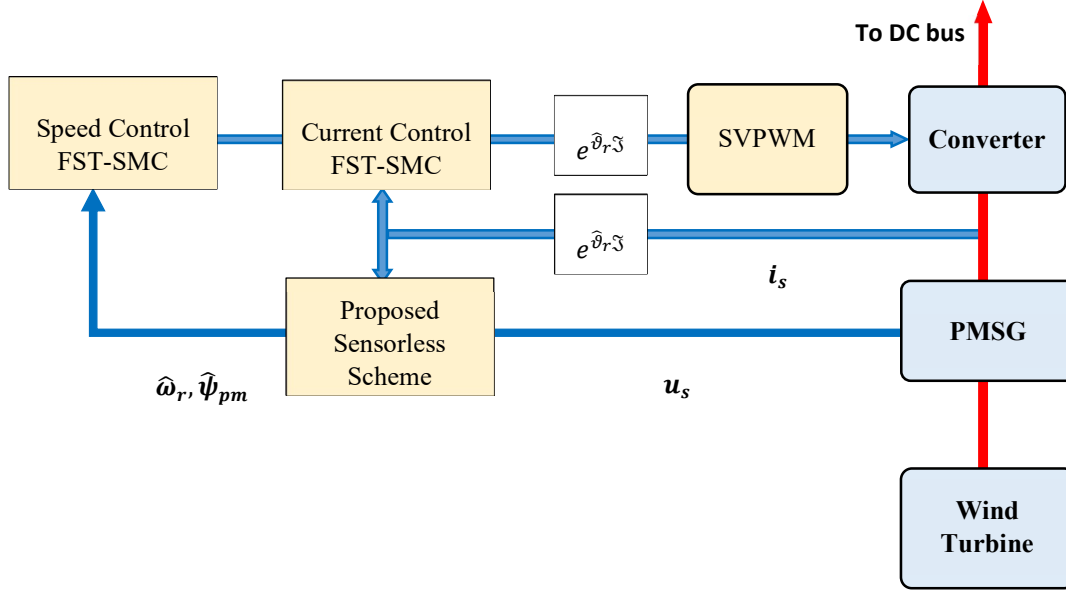


Fig. 1: Block diagram of the stator side control.

### 3.1 Fast-super-twisting sliding mode control

WECSs have highly nonlinear dynamics with variable parameters and are continuously subjected to stochastic wind speeds, which makes conventional PI controllers inappropriate and usually fail to provide satisfactory performance. In this work, a robust non-linear controller based on the Super Twisting Algorithm (STA) is proposed instead of the PI controllers. The author in [37] used the conventional STA in another form for the control of the PMSM. To enhance the tracking of the desired reference and achieve a rapid convergence with better stability, the authors in [38] used the second-order fast terminal SMC to replace the conventional STA applied in [37] while keeping the same structure. This controller is developed in two steps: (i) determine the sliding surface reached by the trajectory of the system and (ii) use the second-order concept to ensure that the control law stays in this surface [38].

The sliding surface is selected as [37]:

$$S_{\omega, i_s} = c_1 \int e_{\omega, i_s} dt + e_{\omega, i_s} \quad (14)$$

With

$$e_{\omega} = \omega_{\text{ref}} - \omega_r \quad (15)$$

$$e_{i_s} = i_{s \text{ref}} - i_s \quad (16)$$

Using equations (7) and (12) with the derivative of equation (14) gives:

$$\frac{de_{\omega}}{dt} = \frac{1}{J} [\Gamma_{em} - \Gamma_L - f\omega_r] + c_1 e_{\omega} \quad (17)$$

$$\frac{de_{i_s}}{dt} = \frac{1}{L} [-(R_s J + n_p \omega_r L_s \mathfrak{J})i_s - n_p \omega_r \psi_{pm} \mathfrak{J} \xi_s + u_s] + c_2 e_{i_s} \quad (18)$$

The conventional form of super-twisting algorithm is defined as:

$$\dot{e}_{\omega, i_s} = u(t) + \zeta \quad (19)$$

Where  $\zeta$  denotes the uncertain disturbance [37].

Since the surface is linear, then the trajectory of the system may take time to reach the equilibrium point, so to accelerate the convergence time, the fast super-twisting control law proposed in [38] is used and is given by:

$$u(t) = u_1 + u_2 \quad (20)$$

Where

$$u_1(t) = -\mathcal{F}\sqrt{|e_{\omega, is}|}\text{sign}(e_{\omega, is}) + \mathcal{F}\mathcal{D}e_{\omega, is} \quad (21)$$

$$u_2(t) = \int -1.5\mathcal{H}\mathcal{D}\sqrt{|e_{\omega, is}|}\text{sign}(e_{\omega, is}) + 0.5\mathcal{H}\text{sign}(e_{\omega, is}) + \mathcal{H}\mathcal{D}^2e_{\omega, is} \quad (22)$$

Where  $\mathcal{F}, \mathcal{D}, \mathcal{H}$  are positive constants. If this condition ( $\dot{S} = S = 0$ ) is verified then the system reaches the sliding surface, therefore, using (17) and (18), the electromagnetic torque and stator voltage can be defined as:

$$\Gamma_{em} = -J[u(t) + \zeta_{\omega}] + \Gamma_L + f\omega_r \quad (23)$$

$$u_s = L[u(t) + \zeta_{is}] - (R_s J + n_p \omega_r L_s \mathfrak{S})i_s - n_p \omega_r \psi_{pm} \mathfrak{S} \xi_s \quad (24)$$

The stability of this controller can be assessed by the following quadratic Lyapunov function [38]:

$$v = Y^T \mathcal{W} Y \quad (25)$$

Where  $Y^T = [u(t)_1/\mathcal{F} \quad u(t)_2]$  and  $\mathcal{W} = \mathcal{W}^T > 0$  is a positive definite matrix, which is defined as:

$$\mathcal{W} = \frac{1}{2} \begin{bmatrix} \mathcal{F}^2 + 4\mathcal{H} & -\mathcal{F} \\ -\mathcal{F} & 2 \end{bmatrix} \quad (26)$$

The derivative of the Lyapunov function is written as:

$$\dot{v} = \dot{Y}^T \mathcal{W} Y + Y^T \mathcal{W} \dot{Y} \quad (27)$$

Substituting equation (26) into equation (27) gives:

$$\dot{v} = \frac{1}{\sqrt{|e|}} [2Y^T M^T + 2\zeta E^T] \mathcal{W} Y \quad (28)$$

Where  $E^T = [0 \quad 1]$ ,  $M^T = \begin{bmatrix} -\mathcal{F} & -\mathcal{H} \\ 1 & 0 \end{bmatrix}$ . The perturbation is assumed bounded such as  $|\zeta| \leq Q$ , then from (28):

$$\dot{v} \leq \frac{1}{\sqrt{|e|}} [2Y^T M^T \mathcal{W} Y + 2\zeta E^T \mathcal{W} Y + Q^2 |\omega| - \zeta^2] \quad (29)$$

Let  $\mathcal{G} = [1 \quad 0]$ , therefore the inequality (29) can be written as:

$$\dot{v} = \frac{1}{\sqrt{|e|}} [2Y^T M^T \mathcal{W} Y + 2\zeta E^T \mathcal{W} Y + Q^2 Y^T \mathcal{G}^T \mathcal{G} Y - \zeta^2] \quad (30)$$

$$\dot{v} \leq \frac{1}{\sqrt{|e|}} [Y^T M^T \mathcal{W} Y + Y^T \mathcal{W} M Y + Q^2 Y^T \mathcal{G}^T \mathcal{G} Y + Y^T \mathcal{W} E E^T \mathcal{W} Y] \quad (31)$$

The inequality (31) can be simplified as:

$$\dot{v} = \frac{1}{\sqrt{|e|}} Y^T [M^T \mathcal{W} + \mathcal{W} M + Q^2 \mathcal{G}^T \mathcal{G} + \mathcal{W} E E^T \mathcal{W}] Y \quad (32)$$

Where  $\mathcal{S} = -(M^T \mathcal{W} + \mathcal{W} M + Q^2 \mathcal{G}^T \mathcal{G} + \mathcal{W} E E^T \mathcal{W})$ , so the Lyapunov function derivative is defined as:

$$\dot{v} \leq -\frac{1}{\sqrt{|e|}} Y^T \mathcal{S} Y \quad (33)$$

$\mathcal{S}$  can be rewritten as:

$$\mathcal{S} = \begin{bmatrix} 3\mathcal{F}\mathcal{H} + \mathcal{F}^3 - \frac{\mathcal{F}^2}{4} - Q^2 & \frac{\mathcal{F}}{2} - \mathcal{H} - \mathcal{F}^2 \\ \frac{\mathcal{F}}{2} - \mathcal{H} - \mathcal{F}^2 & \mathcal{F} - 1 \end{bmatrix} \quad (34)$$

The Lyapunov function derivative is negative and the stability is verified if  $\mathcal{S}$  is positive, this condition is proved if  $\mathcal{F} > 2$ ,  $\mathcal{H} > \frac{\mathcal{F}^3 + \mathcal{Q}^2(4\mathcal{F} - 8)}{\mathcal{F}(4\mathcal{F} - 8)}$  and  $\mathcal{D} > 0$

An approximation of the convergence time of the system (20) to the origin is defined as:

$$t = 2\sqrt{v}/\sigma(\mathcal{S}, \mathcal{W}), \quad \text{where } \sigma(\mathcal{S}, \mathcal{W}) = \lambda_{\min}(\mathcal{S})/\sqrt{\lambda_{\max}(\mathcal{W})}.$$

Where  $\lambda_{\min}(\mathcal{S})$  and  $\lambda_{\max}(\mathcal{W})$  are the minimum and maximum eigenvalues of  $\mathcal{S}$  and  $\mathcal{W}$  respectively.

#### 4. Design of the Sensorless Scheme

The sensorless control scheme is based on the combination of two types of observers, one complementing the other to provide accurate information on the speed and rotor flux. Fig. 2 illustrates the structure of the proposed observer. The first observer generates the speed and has  $i_{\alpha\beta}$ ,  $u_{\alpha\beta}$  as inputs, while the second observer estimate the flux and has  $i_{dq}$ ,  $u_{dq}$  as inputs.

##### 4.1. Speed observer

The nonlinear observer proposed in [4] has several advantages such as a robustness, simplicity, and ease of implementation. Since the observer depends on the permanent magnet flux, therefore it is important to have an accurate flux value to estimate the position correctly. The permanent magnet flux is determined from the flux observer. Lyapunov theory is used to assess the stability of this observer.

Equation (7) describing the model of the NSP-PMSG can be take the following form:

$$L \frac{di_s}{dt} = -R_s i_s + \hat{\omega}_r \psi_{pm} (-\sin \hat{\vartheta}_r + j \cos \hat{\vartheta}_r) - u_s \quad (35)$$

Where

$$\begin{cases} i_s = i_\alpha + j i_\beta \\ u_s = u_\alpha + j u_\beta \end{cases} \quad (36)$$

The design of this observer requires the introduction of a new variable  $x$ , which is given by:

$$x = L i_s + \hat{\psi}_{pm} e^{j\hat{\vartheta}_r} \quad (37)$$

Where  $\hat{\psi}_{pm}$  is the estimated flux delivered by the flux observer, which is detailed in the next section, and the vector is defined as:

$$e^{j\hat{\vartheta}_r} = \cos \hat{\vartheta}_r + j \sin \hat{\vartheta}_r \quad (38)$$

Where  $j$  denotes the complex number ( $j^2 = -1$ ).

The measurement vector expressed in the frame linked to the stator is written as follows:

$$y = -R_s i_s - u_s \quad (39)$$

This vector relies on the current and voltage measurements. From (35), (37) and (39), it can be shown that:

$$\dot{x} = L_s \frac{di_s}{dt} - \hat{\psi}_{pm} \frac{de^{j\hat{\vartheta}_r}}{dt} = y \quad (40)$$

$$\frac{dx}{dt} = L \frac{di_s}{dt} - \hat{\omega}_r \hat{\psi}_{pm} (-\sin \hat{\vartheta}_r + j \cos \hat{\vartheta}_r) = y \quad (41)$$

An additional vector  $\eta(x)$  is introduced into the system, and is expressed in the following form:

$$\eta(x) = x - L i_s \quad (42)$$

Comparing (42) with (37), the Euclidean norm of  $\eta(x)$  can be expressed as:

$$\|\eta(x)\|^2 = \hat{\psi}_{pm}^2 \quad (43)$$

Thus, the dynamic model can be described as:

$$\begin{cases} \dot{\hat{x}} = y \\ z = h(x, y) \end{cases} \quad (44)$$

With

$$h(x, y) = \|\eta(x)\|^2 \quad (45)$$

So, the equation of the nonlinear observer is written as [4, 6]:

$$\dot{\hat{x}} = y + \frac{\kappa_{ob}}{4} \nabla_x h(\hat{x}, t) [z - h(\hat{x}, t)] \quad (46)$$

Where  $\kappa_{ob}/4 > 0$  is the observer gain and  $\nabla$  denotes the gradient operator.

Equation (37) can be determined from (45) as:

$$\nabla_{\hat{x}} h(\hat{x}, t) = 2\eta(\hat{x}) \quad (47)$$

In addition, we can write:

$$z - h(\hat{x}, t) = \|\eta(x)\|^2 - \|\eta(\hat{x})\|^2 \quad (48)$$

Substituting equations (47) and (48) into (46), the derivative of vector  $x$  can be obtained as:

$$\dot{\hat{x}} = y + \frac{K_{ob}}{2} \eta(\hat{x}) [\hat{\Psi}_{pm}^2 - \|\eta(\hat{x})\|^2] \quad (49)$$

Integrating (49) yields the estimated variable  $\hat{x}$ :

$$\hat{x} = \int_0^t \left( y + \frac{K_{ob}}{2} \eta(\hat{x}) [\hat{\Psi}_{pm}^2 - \|\eta(\hat{x})\|^2] \right) dt + \hat{x}_0 \quad (50)$$

Using equation (37), the rotor position estimate is obtained as [39]:

$$e^{j\hat{\theta}_r} = \frac{1}{\hat{\Psi}_{pm}} (\hat{x} - Li_s) \quad (51)$$

The observer gain will be determined using GA optimization as discussed in the next section.

#### 4.1.1 Principle of genetic algorithms (GA) optimization

GA provides solutions to optimization problems that cannot be solved analytically in reasonable time. GA is generally based on three main steps: reproduction, crossover, and mutation. A population of more or less good solutions (genotypes) are randomly created and is then subjected to a process to assess the relevance of the solutions simulating the evolution of species. The most "suitable" solutions to the problem are those which are most likely to survive as the population evolves through successive generations by crossing the best solutions between them and by mutating them [25]. This process is iterated a certain number of times until the final optimal solution is reached [40, 41]. Fig. 2 illustrates a basic flow-chart of GA optimization.

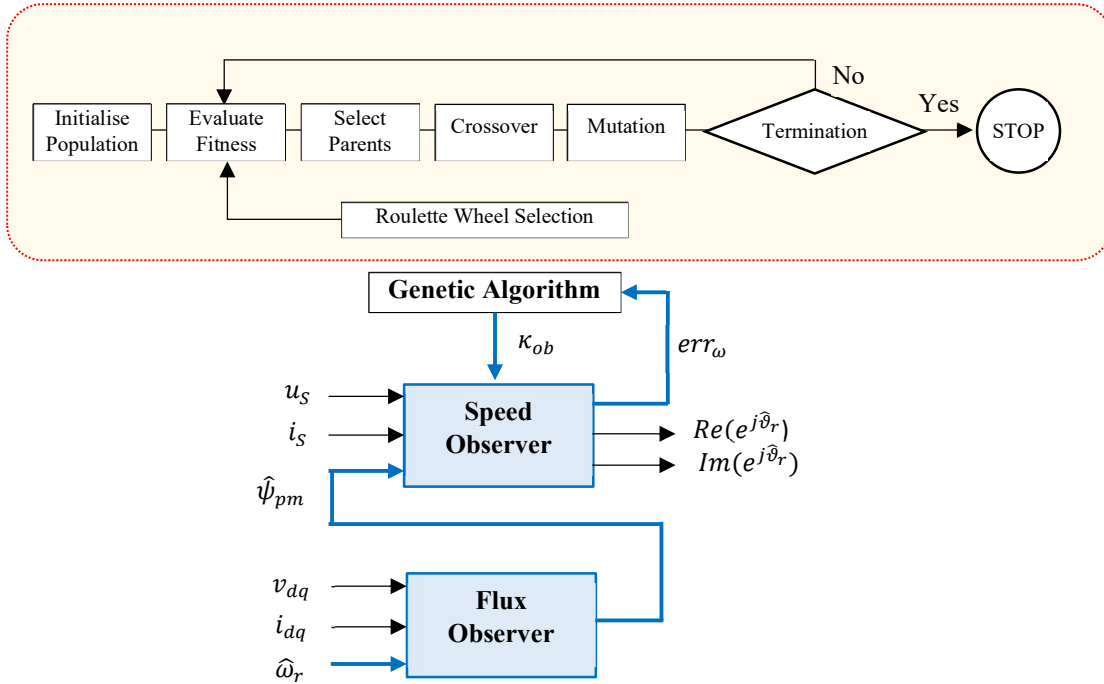


**Fig. 2 :** Block diagram of the GA-optimised sensorless scheme.

Fitness evaluation is an important step in GA. It determines the survival ability of chromosome. In this work, the fitness function is defined as the minimization of the squared speed error, and is given by the following objective function:

$$J = \sum \|e_\omega\|^2 \quad (52)$$

GA selects the best value of the observer gain which minimizes the cost function J [23].

#### 4.1.2 Proposed speed estimation method

Some authors used a PI regulator to reconstruct the speed from the error between the speed integrator and the observer position [4-8]. This paper proposes an effective method to estimate the speed as illustrated in Fig. 3. The speed is extracted from a modified Phase Locked Loop (PLL) introduced in [42].

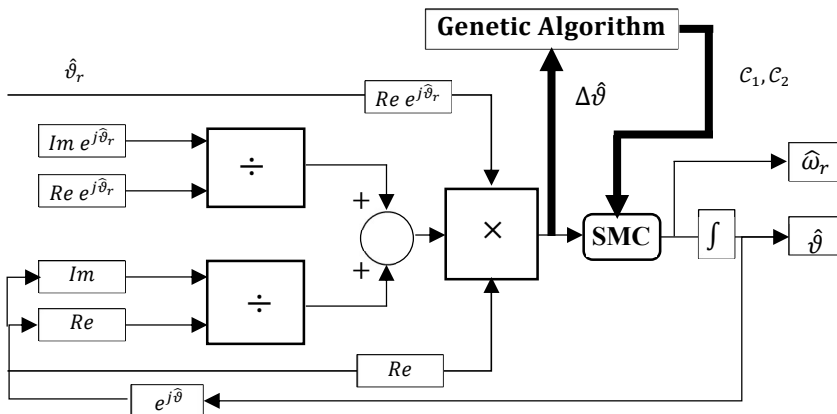


**Fig. 3 :** Block diagram of the proposed speed estimation.

There are typically three equilibrium points in the phase trajectory of a conventional PLL namely  $(0,0)$ ,  $(\pi, 0)$  and  $(-\pi, 0)$ . For positive speeds the point  $(0,0)$  is stable and  $(\pi, 0)$  and  $(-\pi, 0)$  are saddle points. However, for negative speeds, the saddle points become stable points and the stable point becomes a saddle point. In which case the system generates a position estimation error of  $180^\circ$  [43]. In the case of a PMSG, this problem is avoided because the generator spins in one direction only, so the stable point does not change. Therefore, the PLL is introduced without causing any stability problem which is an advantage for the proposed system.

Since the speed observer gives the real and imaginary parts as shown in Fig. 2, therefore, using the proposed PLL circuit, the speed can be extracted from these two parts and the position error can be determined as:

$$\text{Im } e^{j\Delta\hat{\theta}} = \left( \frac{\text{Im}(e^{j\hat{\theta}_r})}{\text{Re}(e^{j\hat{\theta}_r})} - \frac{\text{Im } e^{j\hat{\theta}}}{\text{Re } e^{j\hat{\theta}}} \right) * \text{Re}(e^{j\hat{\theta}_r}) * \text{Re } e^{j\hat{\theta}} \quad (53)$$

Since  $\Delta\hat{\theta}$  is very small, the following approximation holds:

$$\text{Im } e^{j\Delta\hat{\theta}} \cong \Delta\hat{\theta} \quad (54)$$

The closed-loop transfer function of the PLL circuit is given by:

$$H = \frac{k_p s + k_i}{s^2 + 0.5k_p s + 0.5k_i} \quad (55)$$

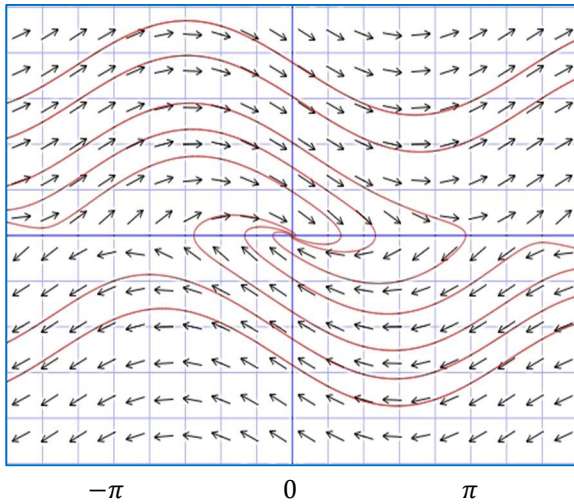
Where  $k_p$ ,  $k_i$  are the proportional and integral gains of the PI regulator. From (55), it is clear that this PLL is similar to a low pass filter. Therefore, the harmonics can be filtered [43].

The proposed PLL scheme can be expressed as follows:

$$s e_{\theta} = e_{\omega} \quad (56)$$

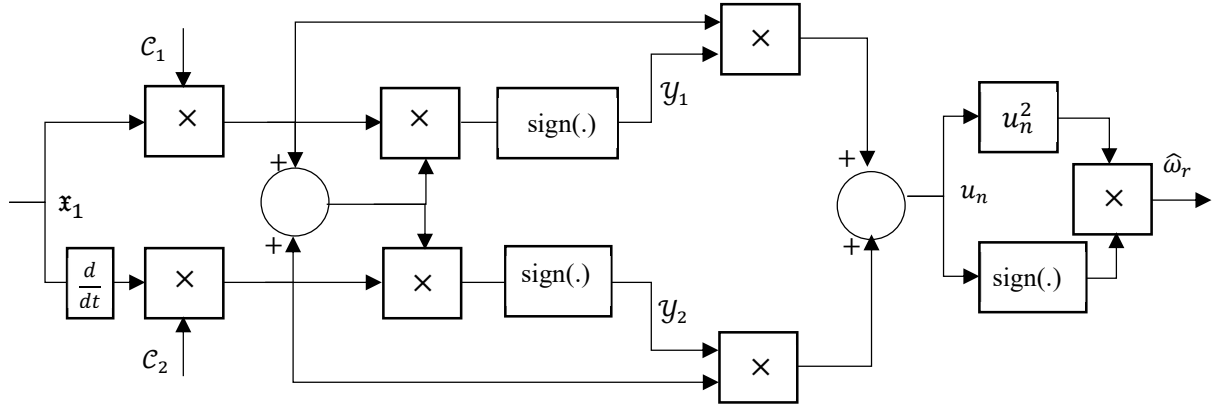
$$s e_{\omega} = -K_p \text{Re}(e_{\theta}) e_{\omega} - K_i \text{Im}(e_{\theta}) \quad (57)$$

Fig. 4 shows the phase plan of the proposed PLL. From this plot it can be observed that the error of the estimated position converges to the equilibrium point  $(0, 0)$ , which satisfies the desired performance of the system.



**Fig.4:** Phase plane of the proposed PLL.

An accurate estimate of the speed requires a robust regulator such as the SMC which is insensitive to parameter variations and is easy to implement.



**Fig. 5:** Block diagram of the SMC.

The proposed SMC is adapted from [44] and its structure is depicted in Fig. 5. The state variable  $\mathfrak{x}_1, \mathfrak{x}_2$  represent the position error and its derivative:

$$\mathfrak{x}_1 = \Delta \hat{\vartheta}_r \quad (58)$$

$$\mathfrak{x}_2 = \dot{\mathfrak{x}}_1 \quad (59)$$

The switching terms are given by:

$$y_1 = \text{sign}((c_1 \mathfrak{x}_1 + c_2 \mathfrak{x}_2) c_1 \mathfrak{x}_1) \quad (60)$$

$$y_2 = \text{sign}((c_1 \mathfrak{x}_1 + c_2 \mathfrak{x}_2) c_2 \mathfrak{x}_2) \quad (61)$$

Where  $(c_1, c_2)$  are positive constants. The control law can be written as:

$$u_n = y_1 * c_1 \mathfrak{x}_1 + y_2 * c_2 \mathfrak{x}_2 \quad (62)$$

Finally, the speed is obtained as:

$$\hat{\omega}_r = \text{sqr}(u_n) * \text{sign}(u_n) \quad (63)$$

To reduce the impact of system uncertainties while still satisfying the robustness condition, the gains  $(c_1, c_2)$  of the SMC must be optimized using the GA technique presented in the previous section. The minimization of the error is the main objective of the fitness function.

The fitness function is defined as follows [23]:

$$j = \sum \|\text{sqr}(\mathfrak{x}_1)\| \quad (64)$$

#### 4.1.3. Stability analysis of the speed observer

The observation error is defined as  $\tilde{x} = \hat{x} - x$ , so the derivative of this error is given by:

$$\dot{\tilde{x}} = -K_{\text{ob}} a(\tilde{x}, t) \left( \tilde{x} + \hat{\Psi}_{\text{pm}} \begin{bmatrix} \cos \hat{\vartheta}_r(t) \\ \sin \hat{\vartheta}_r(t) \end{bmatrix} \right) \quad (65)$$

With:

$$a(\tilde{x}, t) = \frac{1}{2} \|\tilde{x}\|^2 + \hat{\Psi}_{\text{pm}} [\tilde{x}_1 \cos \hat{\vartheta}_r(t) + \tilde{x}_2 \sin \hat{\vartheta}_r(t)] \quad (66)$$

Three cases of stability can be considered [5, 34], which are confirmed by the previous equation (66) and detailed as follows:

**(i) Global stability:** for random speed, all trajectories converge inside the disk given by:

$$\|\tilde{x}\| \leq 2\hat{\Psi}_{\text{pm}} \quad (67)$$

Therefore, this disk is globally attractive.

**(ii) Local exponential stability:** if there exist constants  $T$  and  $\Delta > 0$  such that:

$$\frac{1}{T_s} \int_t^{t+T_s} \hat{\omega}_r^2(s) ds \geq \Delta \quad (68)$$

The equilibrium point  $\tilde{x} = 0$  of (66) is exponentially stable.

### (iii) Stability in regulation

The origin  $\tilde{x} = 0$  is the unique equilibrium point of (66) and is asymptotically stable if there is a constant, non-zero velocity, which verifies the following condition:

$$|\hat{\omega}_r| > \frac{1}{4} K_{ob} \hat{\psi}_{pm}^2 \quad (69)$$

The accuracy of this observer gain is very important; therefore GA is used to determine the optimal gain.

## 4.2. Flux observer

High temperatures and parameter degradation of permanent magnet can cause demagnetization of the machine. This problem can compromise the accurate estimation of the position and may cause instability of the overall control system. For this reason, it is necessary to know the value of flux during operation.

An effective way to identify the flux is the sensorless method. The design of this flux observer is simple, does not require a great deal of computation time and does not need any steady-state requirement. Moreover, it can be used both in salient and non-salient pole PMSG [45]. The mathematic model of non-salient pole PMSG can be formulated as follows:

$$u_s = -R_s i_s + (sJ + \hat{\omega}_r \mathfrak{J}) \psi_s \quad (70)$$

The flux is divided in two terms:

$$\psi_s = \psi_i + \psi_{pm} \quad (71)$$

With

$$\psi_s = [L_s J] i_s \quad (72)$$

Where  $J$  is a  $2 \times 2$  unity matrix  $J = \begin{bmatrix} 1 & 1 \\ 1 & 1 \end{bmatrix}$ .

The derivative of the permanent flux is written as:

$$\frac{d}{dt} \psi_{pm} = \hat{\omega}_r \mathfrak{J} \psi_{pm} \quad (73)$$

Substituting (71) and (73) into (70) gives:

$$u_s + R_s i_s - \frac{d}{dt} \psi_i = \hat{\omega}_r \mathfrak{J} \psi_{pm} \quad (74)$$

The final equations of this observer can be written as:

$$\frac{d}{dt} \tilde{\psi}_s = \gamma(u_s + R_s i_s) + \hat{\omega}_r [J - \gamma] \mathfrak{J} \hat{\psi}_{pm} \quad (75)$$

$$\hat{\psi}_{pm} = \tilde{\psi}_s - \gamma \psi_i \quad (76)$$

Where  $\gamma = (\mathfrak{K}_1 J - \text{sign}(\hat{\omega}_r) \mathfrak{K}_2 \mathfrak{J})$ ,  $\mathfrak{K}_1, \mathfrak{K}_2$  are positive constants and represent the gain of the observer.

To analyze the convergence of the observer, equation (76) is substituted into (75):

$$s \hat{\psi}_{pm} = \gamma [s \psi_i + u_s + R_s i_s - \hat{\omega}_r \mathfrak{J} \psi_{pm}] + \hat{\omega}_r \mathfrak{J} \hat{\psi}_{pm} \quad (77)$$

Using (73) and (74), equation (77) becomes:

$$s(\hat{\psi}_{pm} - \psi_{pm}) = -\hat{\omega}_r \gamma \mathfrak{J} (\hat{\psi}_{pm} - \psi_{pm}) + \hat{\omega}_r \mathfrak{J} (\hat{\psi}_{pm} - \psi_{pm}) \quad (78)$$

Equation (78) can be simplified as:

$$s(\hat{\psi}_{pm} - \psi_{pm}) = (1 - \gamma) \hat{\omega}_r \mathfrak{J} (\hat{\psi}_{pm} - \psi_{pm}) \quad (79)$$

Then, substituting  $\gamma$  with its values yields:

$$s(\widehat{\Psi}_{pm} - \Psi_{pm}) = [(1 - \mathfrak{K}_1 \mathcal{J}) + \text{sign}(\widehat{\omega}_r) \mathfrak{K}_2 \mathfrak{J}] \widehat{\omega}_r \mathfrak{J} (\widehat{\Psi}_{pm} - \Psi_{pm}) \quad (80)$$

Equation (80) can be further simplified into the following form:

$$s(\widehat{\Psi}_{pm} - \Psi_{pm}) = [-\widehat{\omega}_r(-1 + \mathfrak{K}_1 \mathcal{J}) - |\widehat{\omega}_r| \mathfrak{K}_2 \mathfrak{J}] (\widehat{\Psi}_{pm} - \Psi_{pm}) \quad (81)$$

The eigenvalues can be represented as:

$$\begin{bmatrix} \mathcal{L}_1 \\ \mathcal{L}_2 \end{bmatrix} = \begin{bmatrix} -j\widehat{\omega}_r(-1 + \mathfrak{K}_1 \mathcal{J}) - |\widehat{\omega}_r| \mathfrak{K}_2 \\ +j\widehat{\omega}_r(-1 + \mathfrak{K}_1 \mathcal{J}) - |\widehat{\omega}_r| \mathfrak{K}_2 \end{bmatrix} \quad (82)$$

Where  $\mathcal{L}_{1, 2}$  are the conjugate eigenvalues of (81).

From (82) it can be noticed that the real part of the eigenvalues is negative which implies that the estimation error converges to zero [45].

## 5. Simulation results and discussion

The machine parameters used in this simulation study are given in Table 1. To assess the performance and robustness of the proposed observer and control scheme of the WECS, six simulation scenarios are considered.

**Table 1** – Machine parameters used in the simulations.

Parameters	Values	Units
Stator Resistance $R_s$	0.57	$[\Omega]$
Stator Inductance $L$	0.004	$[H]$
Back EMF constant $K_e$	0.078	$[Vs/rad]$
viscous friction $f_v$	0.004	$[Nm \cdot s/rad]$
Rotor flux $\phi_m$	0.064	$[wb]$
Moment of Inertia $\mathcal{J}$	0.002	$[Kg \cdot m^{-2}]$
Number of pole paires $n_p$	2	

### 5.1. Scenario 1: Speed observer with classical PI regulator

Fig. 6 shows the response of the speed and position with their error using PI regulator. It can be observed that the estimated speed matches perfectly the measured value in steady state after 0.1 s. Also, a large error between the measured and estimated position can be noticed from Fig. 6d. Fig.6e shows a poor performance of the flux observer which reaches its nominal value after 1 s and exhibits an overshoot.

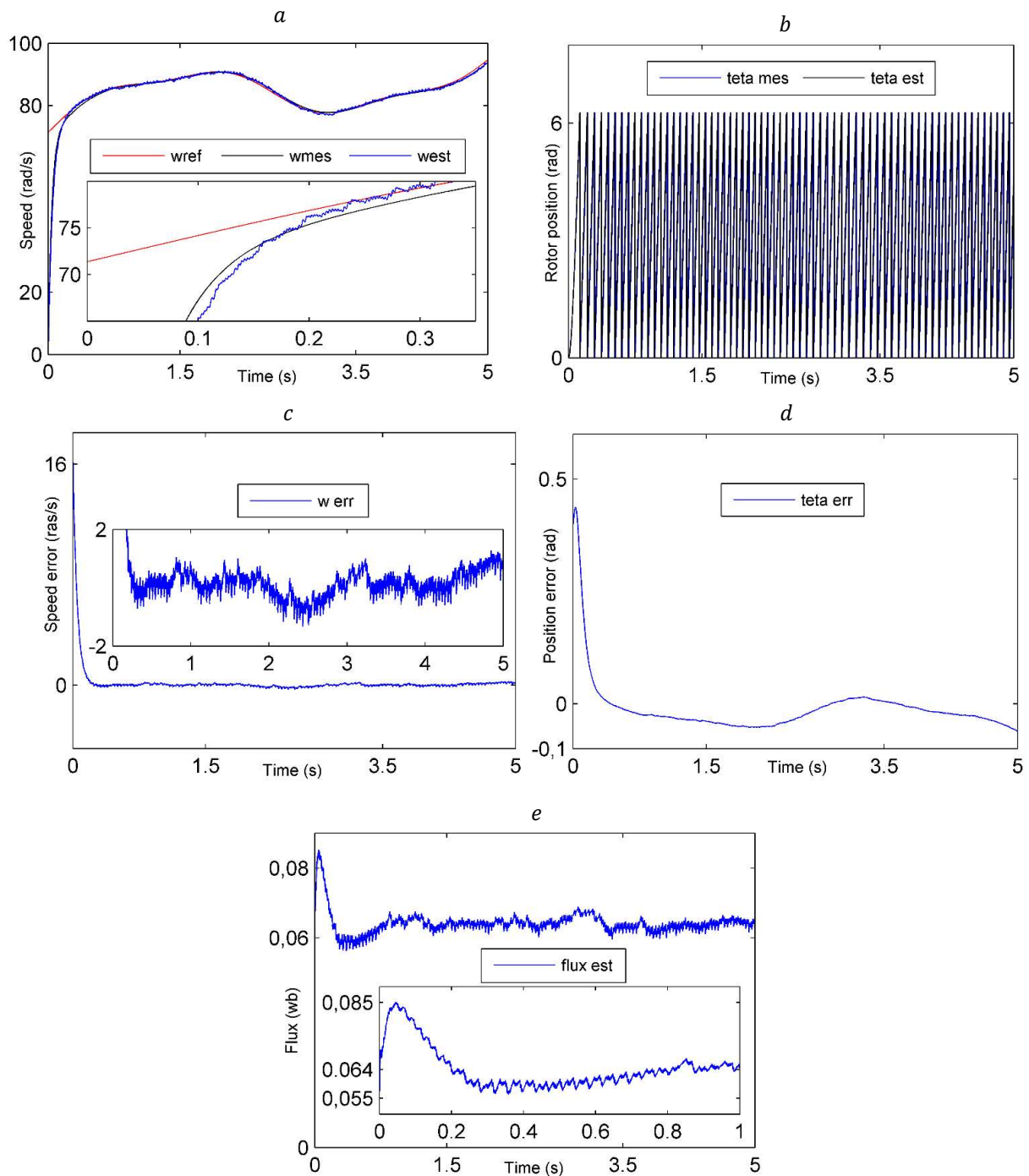


**Fig. 6:** Responses of the a) speed, b) position, c) error of speed, d) error of position, e) flux, using PI with FOC and using PI and speed observer without GA and with flux estimation.

### 5.1. Scenario 2: Speed observer with SMC and FSTSMC regulators

This scenario aims to assess the performance of the proposed controller which includes the FSTSMC applied to the conventional FOC and where SMC is employed in the speed observer. This simulation is performed without optimization and without flux estimation.

From Fig. 7. it can be observed that the estimated and measured speeds match perfectly. Similar results have been obtained for the position with a transient response time of 0.05 s. During speed transients the speed error reaches 12 rad/s and the steady-state speed error is in the range  $[-0.2- 0.2 \text{ rad/s}]$ . In addition, the estimated position error is even smaller in the range  $[0.04- 0.15 \text{ rad}]$ .

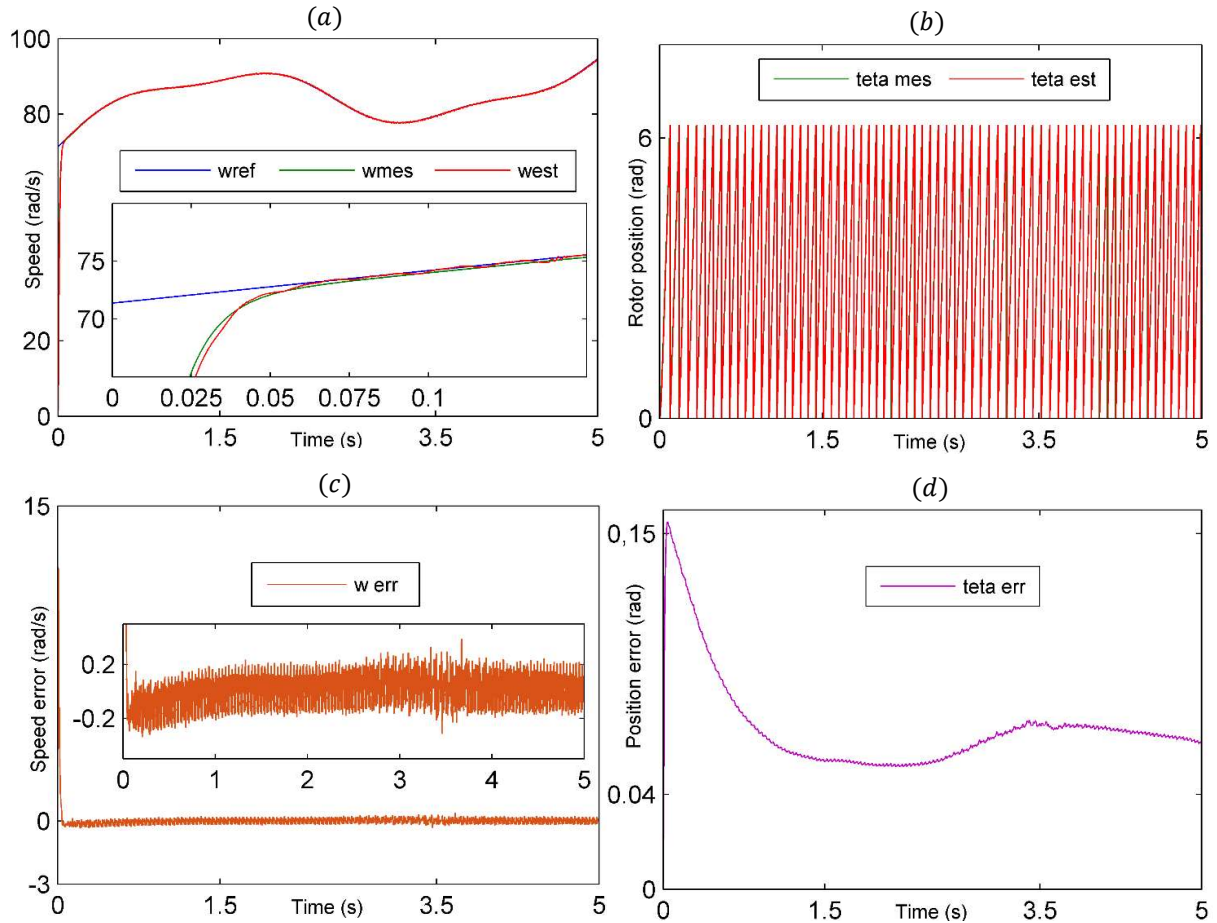


**Fig. 7:** Responses of the a) speed, b) position, c) error of speed, d) error of position using FSTSMC with FOC and using SMC and speed observer without GA and without flux estimation.

### 5.2. Scenario 3: Speed and flux observers with robust SMC and FSTSMC regulators

A similar performance is obtained when flux estimation is introduced in the previous scenario, as shown in Fig.8. During the first 0.025 s period, the speed steady-state error is 13 rad/s, then the error is reduced and assumes values between -0.2 and 0.2 rad/s. The position error is around 0.12 rad. The speed response time is 0.05 s, which is like that obtained in the previous scenario. The estimated flux is ~~much~~ acceptable and does not affect the position estimates. These results show an accurate estimation of the parameters, which demonstrate the effectiveness of the proposed combination of observers.

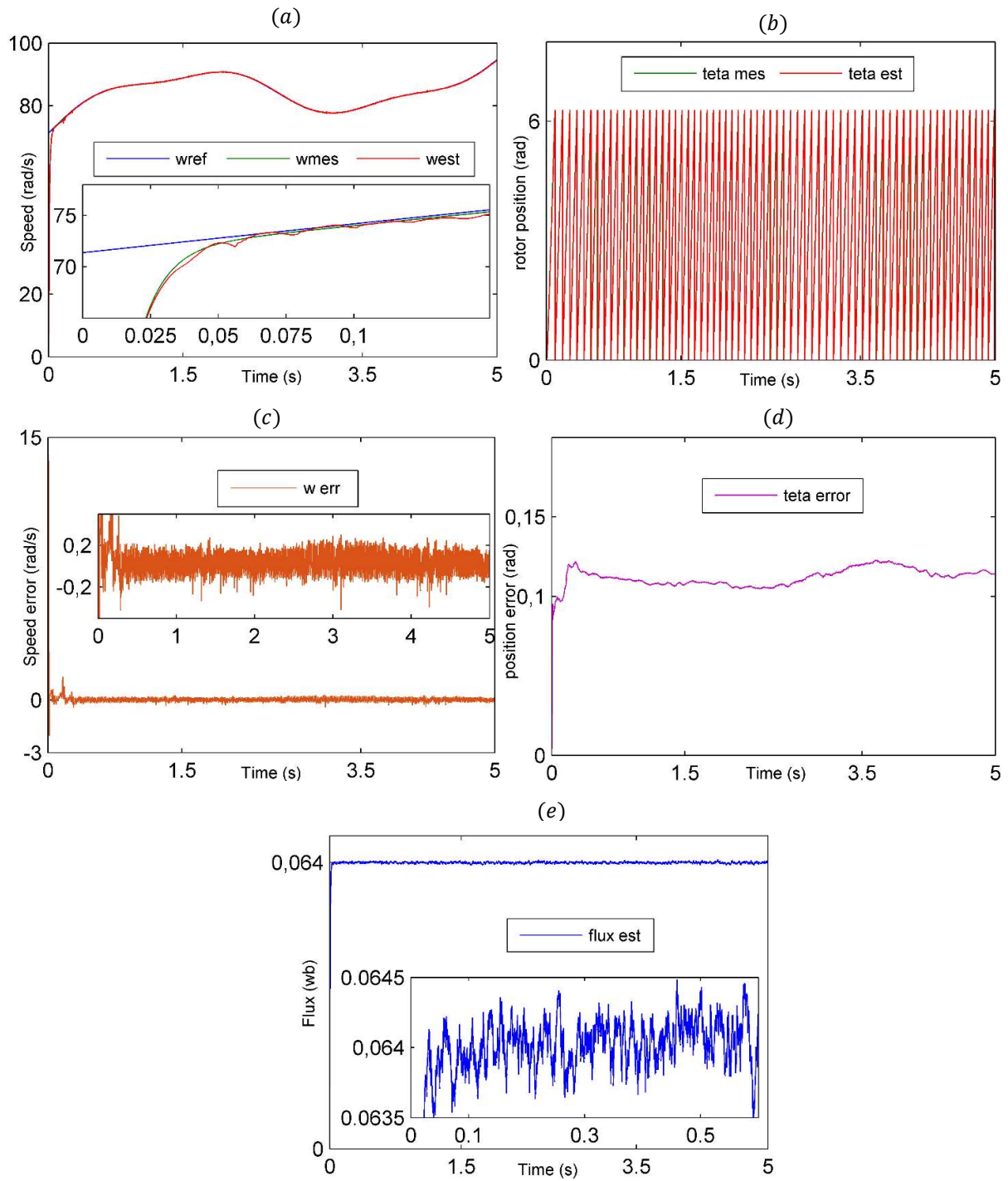


**Fig. 8:** Responses of the a) speed, b) position, c) error of speed, d) error of position, e) flux estimation using FSTSMC with FOC and using SMC and speed observer without GA and with estimation flux.

### 5.3. Scenario 4: Speed observer with robust regulator and optimization algorithm

As shown in Fig. 9, the speed observer based on GA optimization with the measured flux leads to an improved performance with the smallest errors in position (around 0.01 rad) and in speed (varying between -0.1 and 0.1 rad/s). The response time is reduced to  $t_r = 0.012\ s$ . The GA parameters are summarized in Table 2.

**Table 2:** GA parameters.

<b>Parameters</b>	<b>Values</b>
Generations number	50
Population size	100
Mutation rate	0.8
Crossover rate	0.7

As illustrated in Fig. 9 above, by using ITAE as the objective function, the best solution in SMC mode is 36.32, where the optimal gains are  $\mathcal{C}_1 = 4.989$  and  $\mathcal{C}_2 = 2.388$ . For the observer objective function, a better solution of  $4.883e+03$  is achieved which gives an optimal gain of 4.795.

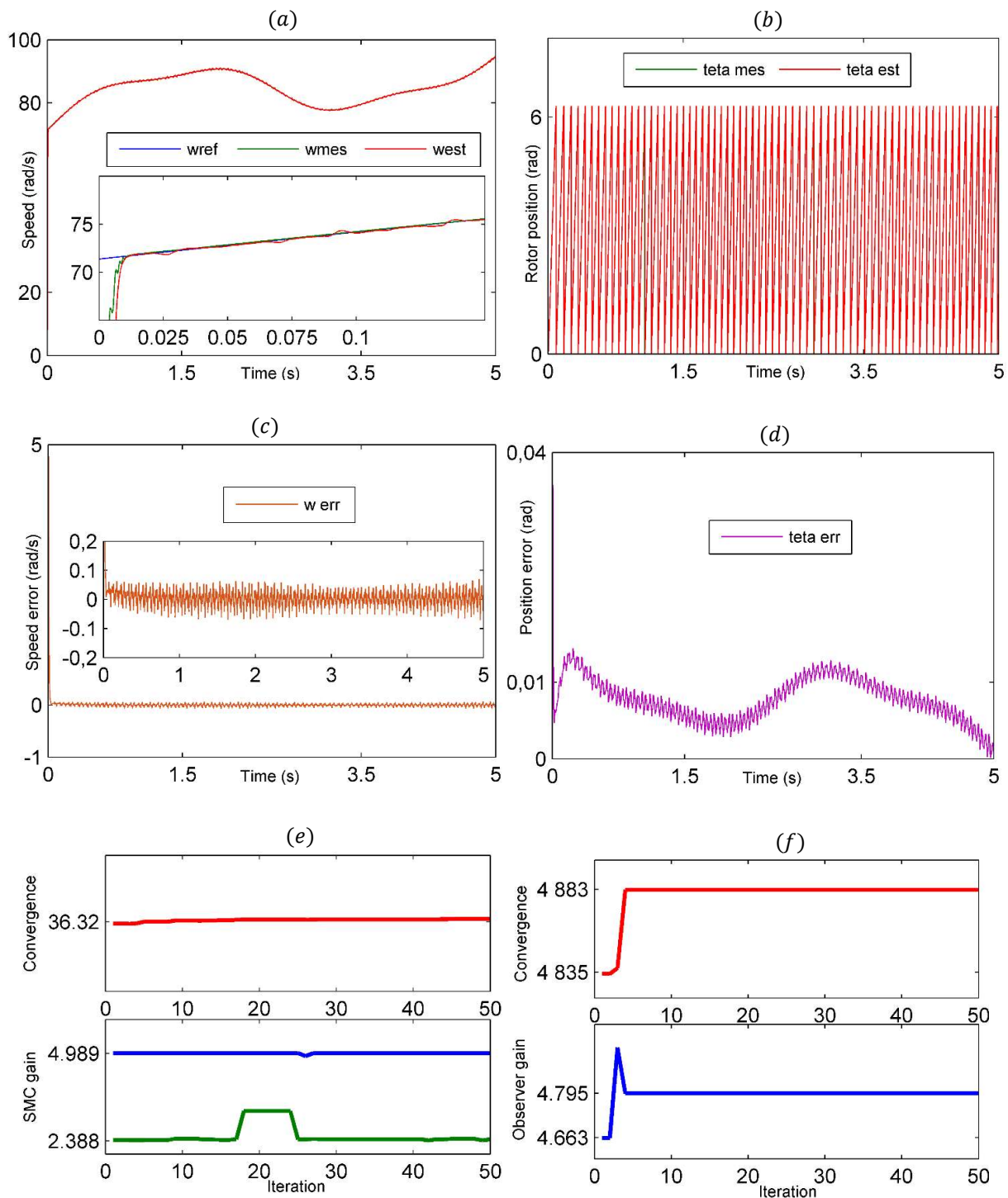


**Fig. 9:** Responses of the a) speed, b) position, c) error of speed, d) error of position, e) gains of SMC, f) gain of observer using FSTSMC with FOC and using SMC and speed observer with GA and without estimation flux.

#### 5.4. Scenario 5: Speed and flux observer with robust SMC and GA optimization.

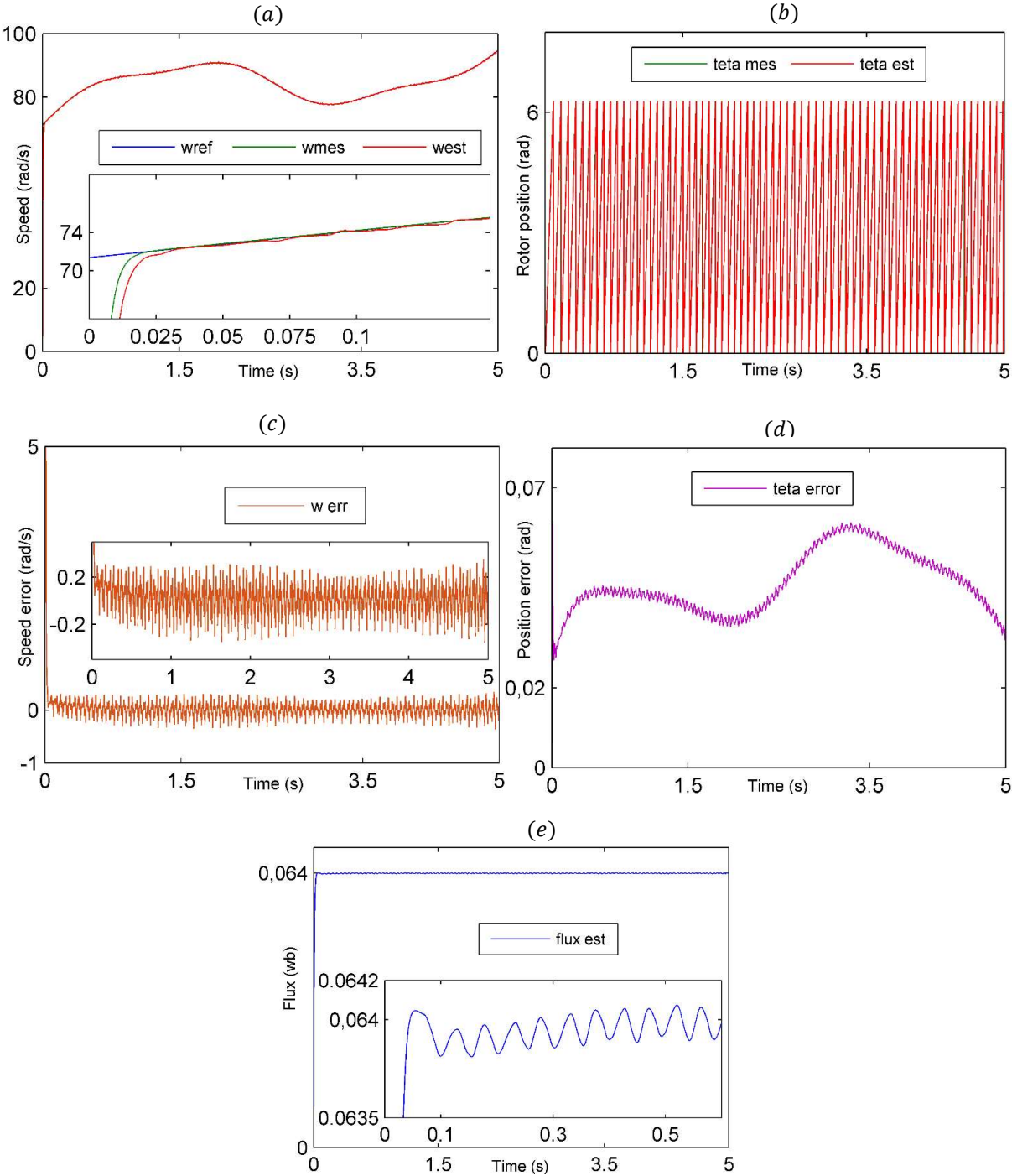
The simulation results of Fig. 10 show a better dynamic performance with GA. The predicted speed is in a good agreement with its measured value. Similar results are achieved for the position. The response time of the speed has reduced to  $t_r = 0.012s$  and the steady-state error of the position decreased to 0.04 rad. The GA improves the performance of flux estimation as demonstrated by the flux waveform depicted in Fig. 10e. Any change exists

between performance of observer with and without flux estimation. In addition, it can be concluded that the SMC with GA has a better response time and good convergence as compared to SMC without GA.

The best solution in SMC mode is 37.21, the new gains of SMC are respectively  $C_1 = 4.9986$  and  $C_2 = 2.401$ . The best solution for the observer is 4900 which generates an optimal gain 3.0318.

In the two methods (Scenarios 3 and 4), 10 generations are enough to ensure the convergence of GA. A very small change of the gain is observed in the presence of estimated flux.

Comparing these results with those obtained in [5, 46] using PI controllers, it can be concluded that the speed and position errors are reduced, therefore the speed of response is improved. In addition, the performance of the PI controllers employed in [5, 46] have not been tested under parameter variations and perturbations.



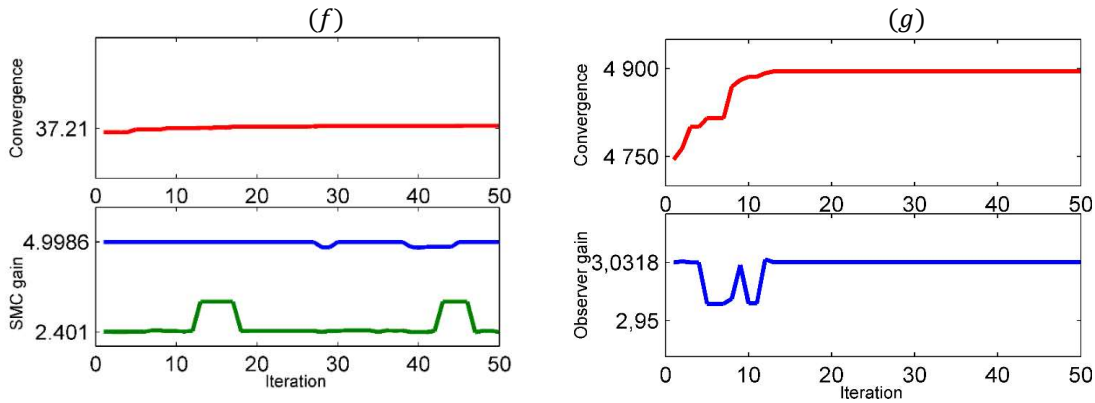


**Fig. 10:** Responses of the a) speed, b) position, c) error of speed, d) error of position, e) estimated flux, f) gains of SMC, g) gain of observer using FSTSMC with FOC and using SMC and speed observer with GA and with flux estimation.

### Scenario 6: Robustness study

The robustness of the proposed control is examined in this scenario. It can be shown from Fig. 11, that the two trajectories in the two-dimensional plane matched by  $S$  and  $\hat{S}$  converge to the origin in a finite time. Furthermore, FSTSMC converges more rapidly than the conventional super twisting sliding mode control (CSTSMC).

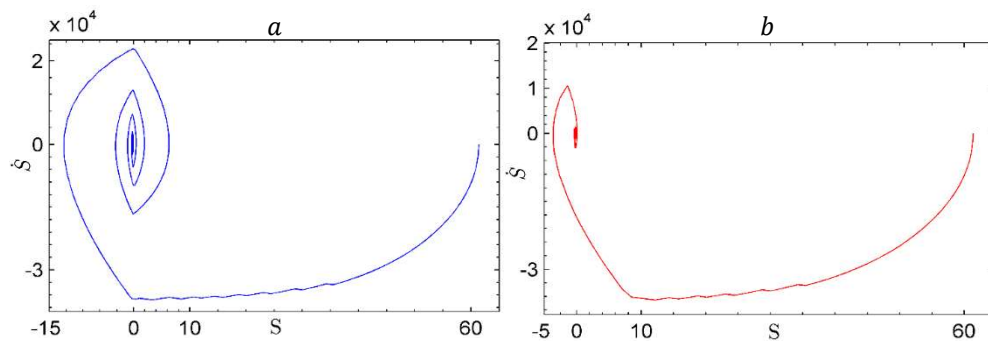


**Fig. 11:** Phase plane trajectory of the controllers a) STSMC, b) FSTSMC.

Fig. 12 illustrates the performance of the controllers under variations of the stator resistance. Three values of the resistance are simulated with PI and FSTSMC. The response of the speed with PI controller for 100% variation of resistance value exhibits a large overshoot. For a variation of 20% and 50% in the stator resistance, the speed is

like the speed obtained under nominal conditions, with a very small overshoot and a small oscillation. As can be observed from Fig. 12, the speed with FSTSMC is not affected by this variation.

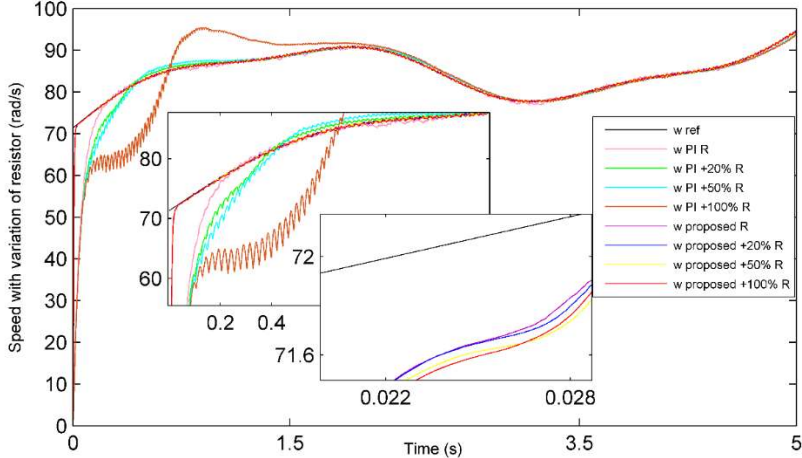


Fig. 12: Response of the speed under resistance variations.

The performance of proposed control system under inductance variations is assessed in Fig. 13. The speed is not affected by the inductance variation with both controllers. However, for the PI controller, some oscillations of the speed around its nominal value can be observed in the case of 100% of inductance variation.

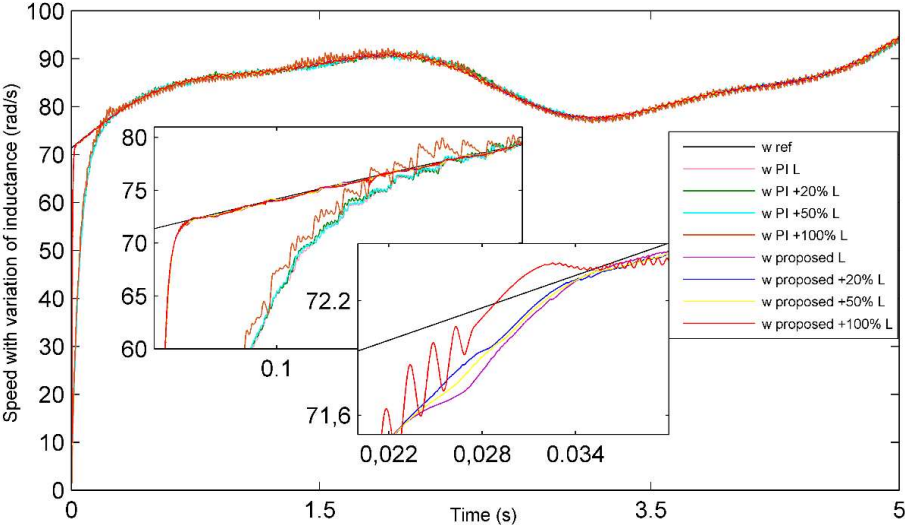
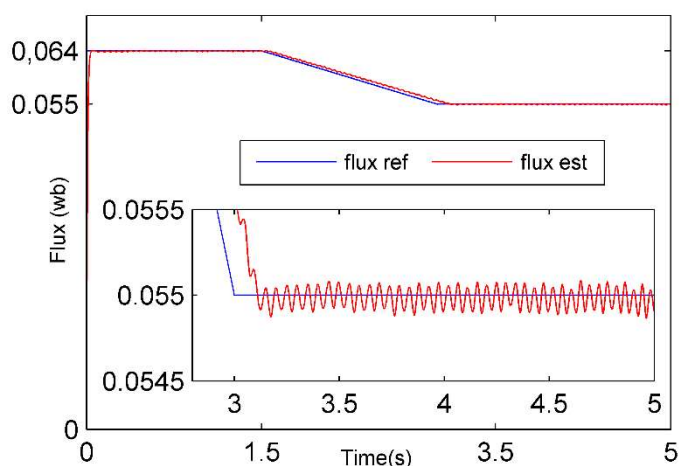


Fig. 13: Speed with inductance variation.

One of the most important features of FSTSMC is its robustness against parameter variation. In Fig. 14, the problem of demagnetization is simulated as a reduction in the flux. It can be observed that the estimated flux coincides with its reference which demonstrates the effectiveness of the proposed scheme under demagnetization.



**Fig. 14:** Test of flux demagnetization.

In the simulation of Fig. 15, a perturbation is applied to the speed between  $t = 2$  s and  $t = 4$  s. The perturbation consists of adding a white noise with sample time 0.01 s and noise power 0.001. With the proposed control scheme, this perturbation did not affect the overall system and the speed perfectly follows its reference as compared to classical PI regulator. The PI controller leads to a larger response time and exhibits a poor tracking performance at the onset of the perturbation.

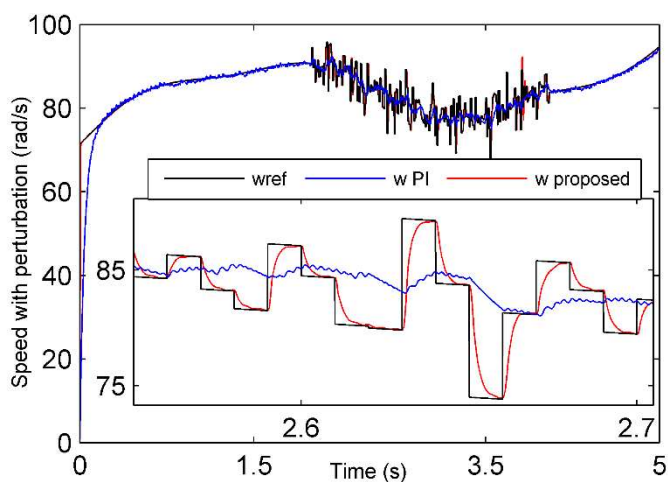


**Fig. 15:** Test of speed perturbation.

The SMC used in the PLL is of order one which suffers from chattering phenomena. Applying GA leads to optimal value of the controller gains, which offers an adaptation between chattering (error) and response time. If the response time increases this will increase the chattering and decrease the precision (i.e. larger error) and vice versa. These results are illustrated in Fig. 16. However, reducing the chattering also leads to a reduction in the transient speed response (i.e. slower response). The FSTSMC is introduced to reduce the response time without affecting the error because it is an SMC of order two, which is known to reduce chattering. The optimal gain obtained by GA gives a very good performance (red signal) and leads to a better compromise between accuracy and speed of response.

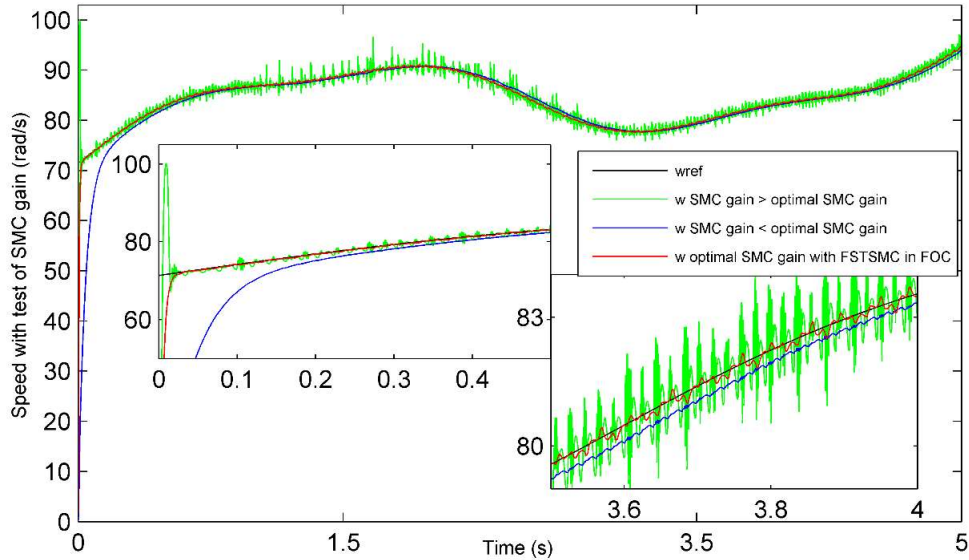


**Fig. 16:** Test of speed with different gains of SMC.

## 6. Conclusion

The proposed sensorless control scheme combining two-observers one for the flux and one for the speed has proved very effective. The flux observer gave an excellent estimation of the Permanent Magnet Synchronous Generator (PMSG) flux where its gain is based on the estimation of the speed. The speed observer estimates the position and speed, and its gain is optimized using Genetic Algorithm (GA). The optimized gain leads to a greater precision and a faster transient response. The Sliding Mode Control (SMC) based on GA optimization is used to determine the speed from the proposed modified PLL using the estimated position and provides an accurate trajectory tracking, which is very well-adapted to the studied system. The ability of the two observers to exchange information has eliminated the demagnetization problem and improved the accuracy of the estimation. The Fast Super Twisting SMC (FSTSMC) was introduced to improve the convergence speed, robustness, and performance of the wind energy conversion system (WECS). To conclude the proposed sensorless control scheme combining the two observers provides greater robustness and stability to the overall Wind Energy Conversion System (WECS).

As future work, we plan to incorporate other optimization algorithms such as Ant Colony optimization for flux observer gain. Even more, the FSTSMC coefficients will not be fixed but varied according to the perturbation.

## Reference

- [1] Roberto Fantino, Jorge Solsona, Claudio Busada, Nonlinear observer-based control for PMSG wind turbine, *Energy* 2016; 113 : 248-57.
- [2] S. Lin, W. Zhang, An adaptive sliding-mode observer with a tangent function-based PLL structure for position sensorless PMSM drives, *Electrical Power and Energy Systems* 2017 ; 88 : 63–74.
- [3] S. K. Kommuri, S. B. Lee, K. C. Veluvolu, Robust Sensors-Fault-Tolerance with Sliding Mode Estimation and Control for PMSM Drives, *IEEE/ASME transactions on mechatronics*, 2018; 23(1) : 17-28.
- [4] R. Ortega, L. Praly, A. Astolfi, J. Lee, K. Nam, Estimation of Rotor Position and Speed of Permanent Magnet Synchronous Motors With Guaranteed Stability, *IEEE Trans. Control. Syst. Technol.* 2011 ; 19(3) : 601 – 14.

- [5] J. Lee, J. Hong, K. Nam, R. Ortega, L. Praly, A. Astolfi, Sensorless Control of Surface-Mount Permanent-Magnet Synchronous Motors Based on a Nonlinear Observer, *IEEE Trans. Power. Electron.* 2010; 25(2) : 290-97.
- [6] A. Khlaief, M. Bendjedia, M. Boussak, M. Gossa, A Nonlinear Observer for High-Performance Sensorless Speed Control of IPMSM Drive, *IEEE Trans. Power. Electron.* 2012; 27(6) : 3028-40.
- [7] A. Bobtsov, A. Pyrkin, R. Ortega, S. N. Vukosavic, A. M. Stankovic, E. V. Panteley, A robust globally convergent position observer for the permanent magnet synchronous motor, *Automatica* 2015; 61 : 47–54.
- [8] J. G. Romero, R. Ortega, Z. Han, T. Devos, F. Malrait, Adaptive flux observer for the permanent magnet synchronous motor, *International Journal of Adaptive Control and Signal Processing.* 2015; 30 : 473–87.
- [9] Xu D, Zhang S, Liu J. Very-low speed control of PMSM based on EKF estimation with closed loop optimized parameters. *ISA Trans*, 2013; 52 : 835–43.
- [10] Y. Shi, K. Sun, L. Huang, and Y. Li, Online identification of permanent magnet flux based on extended Kalman filter for IPMSM drive with position sensorless control, *IEEE Transactions on Industrial Electronics*, 2012; 59(11) : 4169–78.
- [11] A. Arias, X. Rain, and M. Hilairet, Enhancing the flux estimation based sensorless speed control for switched reluctance machines, *Electric Power Systems Research*, 2013; 104 : 62–70.
- [12] X. Xiao, M. Zhang, Y. Li, and M. Li, On-line estimation of permanent magnet flux linkage ripple for PMSM based on a Kalman filter, in *Proc. IECON*, 2006; 1, 1171–75.
- [13] Saman Maroufpoor, RahimAzadnia, OmidBozorg-Haddad, Chapter 17 - Stochastic optimization: stochastic diffusion search algorithm, *Handbook of Probabilistic Models*, 2020; 437-48.
- [14] Zhen-Jun Shi, Jinhua Guo, A new algorithm of nonlinear conjugate gradient method with strong convergence, *computational and applied mathematics*, 2008; 93-106.
- [15] R.P.M. Silva, A.C.B. Delbem, D.V. Coury, Genetic algorithms applied to phasor estimation and frequency tracking in PMU development, *Electrical Power and Energy Systems*, 2013; 44 : 921–29.
- [16] Wenjing Zhang, Bowen Cao, Nan Nan, Mengyue Li, YangQuan Chen, An adaptive PID-type sliding mode learning compensation of torque ripple in PMSM position servo systems towards energy efficiency, *ISA Transactions*, 2020; 110 : 258-70.
- [17] Marek W. Gutowski, biology, physics, small worlds and genetic algorithms, *Leading Edge Computer Science Research*, Warszawa, Poland, 2005; 165-218.
- [18] JH Holland. Genetic algorithms and the optimal allocation of trials. *SIAM J Comput*, 1973; 2(2) : 88–105.
- [19] H. Schewefel. Numerical optimization of computers models. Press, Wiley and sons, Chichester, 1981.
- [20] L.Fogel, A.Owen, M.Walsh, artificial intelligence through simulated evolution, Press, Wiley and sons, new-york city, 1996.
- [21] Mahmut Temel ÖZDEMİR, Dursun ÖZTÜRK, Comparative Performance Analysis of Optimal PID Parameters Tuning Based on the Optics Inspired Optimization Methods for Automatic Generation Control, *Energies* 2017, 10 : 1-19.
- [22] Ching-Chang Wong and Shih-Yu Chang, Parameter Selection in the Sliding Mode Control Design Using Genetic Algorithms, *Tamkang Journal of Science and Engineering*, 1998; 1(2) : 115-22.

- [23] Yi Long, Zhi-jiang Du, Wei-dong Wang, and Wei Dong, Robust Sliding Mode Control Based on GA Optimization and CMAC Compensation for Lower Limb Exoskeleton, Hindawi Publishing Corporation Applied Bionics and Biomechanics; 2016, 1-13.
- [24] Bhawna Tandon, Shiv Narayan<sup>2</sup> and Jagdish Kumar, Sliding Mode Control with Nonlinear Disturbance Observer based on Genetic Algorithm for Inverted Pendulum with Mismatched Disturbances, Indian Journal of Science and Technology, 2017; 10(30) : 1-5.
- [25] L.M. Porter, K.M. Passino, Genetic adaptive observers. Eng. Appl. Artif. Intell. 1995; 8: 261–69.
- [26] X. Yang, Z. Li, D. Boutaib, Parameter and State Estimation for Uncertain Nonlinear Systems by Adaptive Observer Based on Differential Evolution Algorithm, Appl. Sci., 2020; 10 : 1-20.
- [27] Andrzej, P.; Jelonkiewicz, J. Genetic Algorithm for Observer Parameters Tuning in Sensorless Induction Motor Drive. In Neural Networks and Soft Computing; Physica-Verlag HD: Heidelberg, Germany, 2003.
- [28] M. R. Feyzi, M. Shafiei, M. B. Kouhshahi, S. A. KH. Mozaffari Niapour, Position Sensorless Direct Torque Control of Brushless DC Motor Drives Based on Sliding Mode Observer Using NSGA-II Algorithm Optimization, In Farhangi, S (Ed.) Proceedings of the 2nd Power Electronics, Drive Systems and Technologies Conference. IEEE, United States of America, 2011; 151-56.
- [29] A. M. Shotorbania, B.M. Ivatloo, L. Wang, M. Marzband, M. Sabahia, Application of finite-time control Lyapunov function in low-power PMSG wind energy conversion systems for sensorless MPPT, Electrical Power and Energy Systems. 2019; 106: 169–82.
- [30] Shengquan Li, Kezhao Zhang, Juan Li Chao Liu, On the rejection of internal and external disturbances in a wind energy conversion system with direct-driven PMSG, ISA Transactions, 2016; 61: 95-103.
- [31] W. Ayri, M. Ourahou, B. El Hassouni, A. Haddi, Direct torque control improvement of a variable speed DFIG based on a fuzzy inference system, Mathematics and Computers in Simulation, 2020; 167 : 308-24.
- [32] S. Lin, W. Zhang, An adaptive sliding-mode observer with a tangent function-based PLL structure for position sensorless PMSM drives, Electrical Power and Energy Systems 2017; 88 : 63–74.
- [33] Hinkkanen, M. & Tuovinen, T. & Harnefors, L. & Luomi, J. A Combined Position and Stator-Resistance Observer for Salient PMSM Drives: Design and Stability Analysis. IEEE Transactions on Power Electronics. 2012; 27(2) : 601-09.
- [34] Dhruv Shah, Gerardo Espinosa–Perez, Romeo Ortega, Mickael Hilaiet, Sensorless Speed Control of Non–salient Permanent Magnet Synchronous Motors, Proceedings of the 18th World Congress The International Federation of Automatic Control Milano (Italy) August 28 - September 2, 2011, p 11109-14.
- [35] Shan Chai, Liuping Wang, Eric Rogers, Model predictive control of a permanent magnet synchronous motor with experimental validation, Control Engineering Practice 2013; 21 : 1584–93.
- [36] Mihoub Youcef, Toumi Djilali, Sandrine Moreau, Hassaine Said, Daoud Bachir, DSP improvement of a vector speed induction motor control with a RST and adaptive fuzzy controller, Bulletin of Electrical Engineering and Informatics, Vol. 10, No. 3, 2021, 1232-44.
- [37] Hao Chen, Shifeng Tang, Jingang Han, Tianhao Tang, Nadia Aït-Ahmed, Zhibin Zhou, Mohamed Benbouzid, High-order sliding mode control of a doubly salient permanent magnet machine driving marine current turbine, Journal of Ocean Engineering and Science, 2021; 6 (1) : 12-20.
- [38] Lei Zhang, Sibowang, and Jing Bai, Fast-super-twisting sliding mode speed loop control of permanent magnet synchronous motor based on SVM-DTC, IEICE Electronics Express, 2021; 18(1) : 1-6.

- [39] H. Pillai., R. Ortega, M. H. Gomez, T. Devos, F. Malrait, Robustness Analysis of Position Observers for Permanent Magnet Synchronous Motors vis-à-vis Rotor Saliency, 3rd International Electric Drives Production Conference (EDPC), Dec 2013.
- [40] M. Ahmed, M.A. Ebrahim, H.S. Ramadan, M. Becherif, optimal genetic-sliding mode control of VSC-HVDC transmission systems, *Energy Procedia*, 2015; 74 : 1048-60.
- [41] Nedim Tutkun, Genetic estimation of iron losses in strip wound toroidal cores under PWM flux conditions, *Journal of Magnetism and Magnetic Materials* 2006; 300 : 506–18.
- [42] n.ikken, a.bouknadel, a.haddou, hafsa el Omari, hamid el Omari, A comparative Study and implementation of Single-Phase PLL techniques for Grid-Connected Inverters Systems, *Journal Electrical Systems* 2018; 14(4) : 116-33.
- [43] S. Lin, W. Zhang, An adaptive sliding-mode observer with a tangent function-based PLL structure for position sensorless PMSM drives, *Electrical Power and Energy Systems* 2017; 88 : 63–74.
- [44] Ahmed Safa, E.L. Madjid Berkouk, Youcef Messlem, Abdelmadjid Gouichiche, A robust control algorithm for a multifunctional grid tied inverter to enhance the power quality of a microgrid under unbalanced conditions, *Electrical Power and Energy Systems* 2018; 100 : 253–64.
- [45] S. Shinnaka, New sensorless vector control using minimum-order flux state observer in a stationary reference frame for permanent magnet synchronous motors, *IEEE Trans. Ind. Electron.*, 2006; 53(2) : 388–98.
- [46] A. Khlaief, M. Bendjedia, M. Boussak, A. Châari, Nonlinear observer for sensorless speed control of IPMSM drive with stator resistance adaptation, *CCCA12*; 2012.